PNAS BRIEF REPORT | EARTH, ATMOSPHERIC, AND PLANETARY SCIENCES OPEN ACCESS

Rapid shift in methane carbon isotopes suggests microbial emissions drove record high atmospheric methane growth in 2020–2022

Sylvia Englund Michel[a,b,1], Xin Lan[c,d], John Miller[d], Pieter Tans[a], J. Reid Clark[a], Hinrich Schaefer[e], Peter Sperlich[e], Gordon Brailsford[e], Shinji Morimoto[f], Heiko Moossen[g], and Jianghanyang Li[a,b]

Edited by Mark Thiemens, University of California San Diego, La Jolla, CA; received June 19, 2024; accepted September 5, 2024

The growth rate of the atmospheric abundance of methane (CH_4) reached a record high of 15.4 ppb yr^{-1} between 2020 and 2022, but the mechanisms driving the accelerated CH_4 growth have so far been unclear. In this work, we use measurements of the ^{13}C:^{12}C ratio of CH_4 (expressed as $\delta^{13}C_{CH4}$) from NOAA's Global Greenhouse Gas Reference Network and a box model to investigate potential drivers for the rapid CH_4 growth. These measurements show that the record-high CH_4 growth in 2020–2022 was accompanied by a sharp decline in $\delta^{13}C_{CH4}$, indicating that the increase in CH_4 abundance was mainly driven by increased emissions from microbial sources such as wetlands, waste, and agriculture. We use our box model to reject increasing fossil fuel emissions or decreasing hydroxyl radical sink as the dominant driver for increasing global methane abundance.

methane | stable isotopes | greenhouse gases

Methane (CH_4) is the second-most abundant anthropogenic greenhouse gas and has global warming potential (GWP) of 28 over 100 y (1); as a result, CH_4 has consequential near-term radiative effects and is a prominent target for mitigation (2). Following a short pause in growth from 1999 to 2006, both the abundance and growth rate of atmospheric methane have been increasing (3). During 2020–2022, the observed CH_4 growth rate reached a record high since NOAA measurements began in 1983, averaging 15.4 ± 0.6 ppb yr^{-1} (4). Understanding the mechanisms driving this accelerated growth is essential for predicting its future climate impact and providing scientific support for climate mitigation strategies (2).

The carbon isotopic composition of atmospheric CH_4 ($\delta^{13}C_{CH4}$) is a powerful tool for tracking the sources and sinks of atmospheric CH_4. Different CH_4 sources have distinctive $\delta^{13}C_{CH4}$ values: Microbial CH_4 emissions (wetlands, livestock, landfills, etc.) have lower $\delta^{13}C_{CH4}$ values (global mean of –62‰) than pyrogenic (biomass and biofuel burning, global mean of –24‰) and fossil fuel CH_4 emissions (global mean of –45‰) (5). Various sinks of atmospheric CH_4 also have distinctive isotopic effects. Therefore, combined observations of atmospheric CH_4 mole fraction and $\delta^{13}C_{CH4}$ can provide unique constraints on the changes of global CH_4 sources and sinks during the post-2006 rapid CH_4 growth.

The National Oceanic and Atmospheric Administration's Global Monitoring Laboratory (NOAA/GML) has been carefully monitoring the global CH_4 burden through the Global Greenhouse Gas Reference Network (GGGRN) for over four decades. The collaboration between NOAA/GML and the Institute of Arctic and Alpine Research (INSTAAR) at the University of Colorado Boulder has enabled $\delta^{13}C_{CH4}$ measurements from the GGGRN since 1998, currently measuring weekly or biweekly from 22 globally distributed background sites (6). The dataset has been widely used for studying the evolution of global CH_4 sources and sinks (7–9). Here, we report our most recent observations of atmospheric CH_4 mole fractions and $\delta^{13}C_{CH4}$ values through the end of 2022 and then use a box model to examine and quantify the contributions of potential drivers of the record-high CH_4 growth rate.

Results and Discussion

The global average methane growth rates in 2020, 2021, and 2022 reached record levels of 15.2 ± 0.45, 17.9 ± 0.45, and 13.1 ± 0.8 ppb yr^{-1}, significantly higher than the average growth rates of 9.2 ppb yr^{-1} in 2014–2020, and 5.3 ppb yr^{-1} in 2008–2014 (Fig. 1*A*). Meanwhile, we observed the lowest global average $\delta^{13}C_{CH4}$ in the observational record: –47.67 ± 0.01‰ in 2022. The global $\delta^{13}C_{CH4}$ growth rate from 2020–2022 was –0.09 ± 0.01‰ yr^{-1}, a much faster decrease than –0.04 ± 0.02‰ yr^{-1} in 2014–2020 and –0.03 ± 0.02‰ yr^{-1} in 2008–2014 (Fig. 1*A*).

Author affiliations: [a]Institute of Arctic and Alpine Research, University of Colorado, Boulder CO 80303; [b]Department of Atmospheric and Oceanic Sciences, University of Colorado, Boulder CO 80303; [c]Cooperative Institute for Research in Environmental Sciences, University of Colorado, Boulder CO 80309; [d]Global Monitoring Laboratory, National Oceanic and Atmospheric Administration, Boulder CO 80305; [e]Department of Tropospheric Chemistry, National Institute of Water and Atmospheric Research, Wellington 6021, NZ; [f]Graduate School of Science, Tohoku University, Sendai 980-8578, Japan; and [g]Max Planck Institute for Biogeochemistry, Jena 07745, Germany

Author contributions: S.E.M., X.L., J.M., and J.L. designed research; S.E.M., X.L., J.M., J.R.C., and J.L. performed research; S.E.M., X.L., J.M., P.T., J.R.C., H.S., P.S., G.B., S.M., and H.M. contributed new reagents/analytic tools; S.E.M., X.L., J.M., and J.L. analyzed data; and S.E.M., X.L., J.M., P.T., and J.L. wrote the paper.

The authors declare no competing interest.

Copyright © 2024 the Author(s). Published by PNAS. This open access article is distributed under Creative Commons Attribution License 4.0 (CC BY).

[1]To whom correspondence may be addressed. Email: sylvia.michel@colorado.edu.

This article contains supporting information online at https://www.pnas.org/lookup/suppl/doi:10.1073/pnas.2411212121/-/DCSupplemental.

Published October 21, 2024.

Downloaded from https://www.pnas.org by 178.205.55.180 on November 14, 2024 from IP address 178.205.55.180.

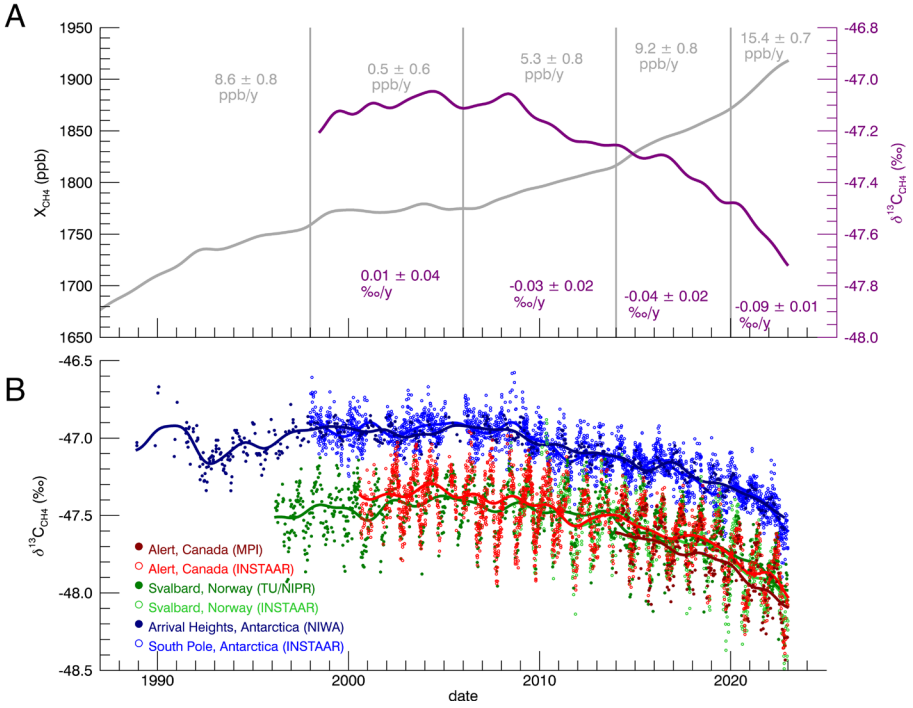

Fig. 1. (*A*) Trend of globally averaged CH_4 abundance (in gray) and $\delta^{13}C_{CH4}$ (purple) from the NOAA/GML GGGRN. Mean growth rates of CH_4 mole fraction and $\delta^{13}C_{CH4}$ are shown for the following time periods: 1983–1998, 1999–2006, 2008–2014, 2014–2020, and 2020–2022. (*B*) Colocated $\delta^{13}C_{CH4}$ measurements at Alert (Canada), Svalbard (Norway), and Antarctica by INSTAAR, NIWA, TU/NIPR, and MPI. Each dataset is fitted with a trend in the same color.

The rapid decrease in $\delta^{13}C_{CH4}$ in 2020–2022 is observed by multiple long-term monitoring programs: Max Planck Institute (MPI), National Institute of Water and Atmospheric Research (NIWA), and Tohoku University and National Institute of Polar Research (TU/NIPR, Fig. 1*B*), which have independent sampling schemes, analytical techniques, and data processing and quality protocols. These observations exhibit similar trends confirming the accelerated decreasing trend in atmospheric $\delta^{13}C_{CH4}$ in 2020–2022 (*SI Appendix*).

To investigate potential drivers for the rapid CH_4 growth, we used a box model (10) to reconstruct the time series of global average CH_4 mole fraction and $\delta^{13}C_{CH4}$. Initial model emissions and sinks prior to 1999 are based on optimized values from a global 3-D inverse model (8) to allow the model to reach steady state with respect to CH_4 mole fractions and $\delta^{13}C_{CH4}$ during 1999 to 2006. We treated the time series as four segments (1999–2006, 2008–2014, 2014–2020, and 2020–2022), each with distinct CH_4 and $\delta^{13}C_{CH4}$ growth rates (Fig. 1*A*). We conducted different simulations to test the isotopic response to possible CH_4 growth drivers (Fig. 2): 1) decreased OH in the troposphere (OH); 2) increased fossil-fuel emissions (FF); 3) increased microbial emission (MICR). In each simulation, we adjusted the flux of each source/sink category in each time segment to match the observed CH_4 growth rate and then compared the resulting simulated atmospheric $\delta^{13}C_{CH4}$ values to our observations.

Our model shows that only the MICR simulation displays a decrease in $\delta^{13}C_{CH4}$. However, increasing only microbial emissions resulted in lower $\delta^{13}C_{CH4}$ than the observations, so we also adjusted fossil fuel emissions to best fit both the observed CH_4 mole fraction and $\delta^{13}C_{CH4}$ (Fig. 2). Our best-fit result of the MICR simulation (*SI Appendix*) required an increase of microbial emissions over the steady state mean by 14 Tg yr^{-1} in 2008 with a concurrent increase in fossil emissions of 10 Tg yr^{-1}; then in 2014, the microbial emissions increased by an additional 22 Tg yr^{-1}, and fossil emissions increased by 3 Tg yr^{-1}. These results are consistent with previous inverse modeling studies (8, 11, 12) that suggested approximately 85% of CH_4 growth during 2007–2020 was due to increased microbial emissions. To capture the rapid growth in CH_4 mole fraction and the decline of $\delta^{13}C_{CH4}$ in 2020–2022, our model suggests an increase in microbial emissions of 32 Tg yr^{-1} in 2020 with no increase in fossil CH_4 emissions required to match observations.

Decreases in biomass burning emissions between 10 to 30% over the past 2 decades (13, 14) could also explain some of the observed changes in $\delta^{13}C_{CH4}$. Such decreases allow for more fossil emissions due to high $\delta^{13}C_{CH4}$ from biomass burning. However, even considering the decreased biomass burning emissions, our model still suggests the post-2020 CH_4 growth is almost entirely driven by increased microbial emissions (*SI Appendix*). Likewise, we modeled 1) a small

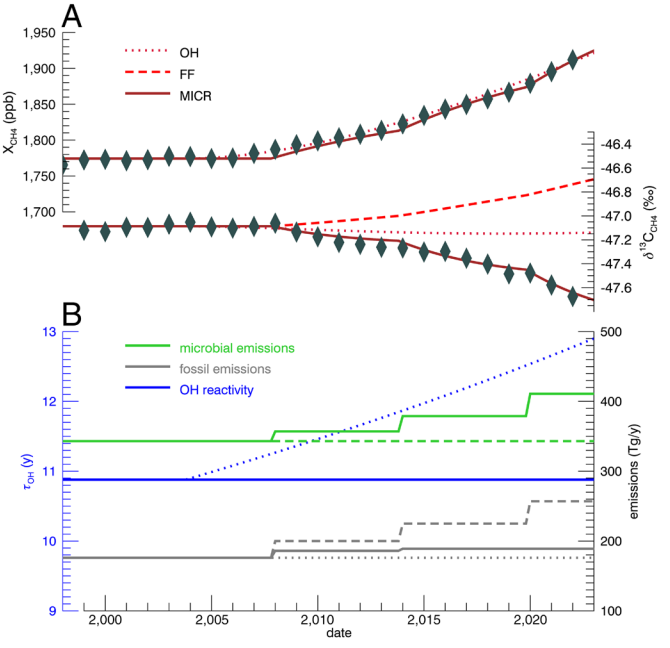

Fig. 2. (*A*) Modeled response of CH_4 mole fraction and $\delta^{13}C_{CH4}$ due to different CH_4 growth drivers. (*B*) Emissions and CH_4 lifetime relative to OH for each scenario.

Downloaded from https://www.pnas.org by 178.205.55.180 on November 14, 2024 from IP address 178.205.55.180.

increasing trend in OH number density (15), 2) an alternate OH fraction factor, and 3) a more negative $\delta^{13}C_{CH4}$ value of fossil fuel emissions. In all scenarios, emission increases dominated by microbial sources are required to track both atmospheric CH_4 and $\delta^{13}C_{CH4}$ (*SI Appendix*). In this underconstrained problem, there are many ways to adjust model parameters to fit the model to the atmospheric data; however, all of the reasonable solutions require very large increases in microbial emissions. (An example of an unrealistic scenario would be an extreme case where biomass burning emissions decline to zero by 2020; only then do fossil fuel emission increases become comparable to those from microbial sources.)

Atmospheric $\delta^{13}C_{CH4}$ does not allow us to differentiate between anthropogenic microbial sources (livestock, landfills) and natural ones (wetlands), so further study is necessary to investigate the potential climate feedback hypothesis (16). However, our box model suggests that microbial emissions played an even more significant role during 2020–2022 than in the years since 2008, which is in general agreement with studies that emphasize the key role of wetland emission increases to the recent global CH_4 budget (11, 12, 17, 18).

Materials and Methods

Atmospheric $\delta^{13}C_{CH4}$ of background air samples collected from the GGGRN are measured using an Isotope Ratio Mass Spectrometer equipped with a custom-built extraction system which traps methane from whole air, focuses the sample, separates it from other carbon-containing compounds, combusts it to CO_2, and measures it relative to a standard (6). Data extension and integration techniques were used to convert global measurements of CH_4 and $\delta^{13}C_{CH4}$ from the GGGRN into global averages and growth rates.

We used a two-box model with time steps of 0.2 y to investigate changes in sources and sinks that could match our observations of CH_4 and $\delta^{13}C_{CH4}$. The box model specifies CH_4 emissions from microbial, fossil, and pyrogenic sources with prescribed $\delta^{13}C$ values of –61.7‰, –44.8‰, and –24.3‰, respectively (5). Sinks include uptake by soil microbes, and oxidation by OH, Cl, and $O(^1D)$, all of which have associated kinetic isotope fractionation factors. The model was tuned to match observations from 1999–1996 and then adjusted to test the isotopic effects of different source/sink scenarios. More details are available in *SI Appendix*.

Data, Materials, and Software Availability. Data have been deposited in NOAA Global Monitoring Laboratory Data Repository (https://doi.org/10.15138/JQEV-PF31) (19).

ACKNOWLEDGMENTS. We thank the people around the world who support NOAA's GGGRN, NOAA GML personnel Monica Madronich and Eric Moglia, and INSTAAR Stable Isotope lab team members Kerstin Braun, John Ortega, Taline Leon, and Bruce Vaughn. INSTAAR's Stable Isotope Lab is funded in part by NOAA GML. This research was also partially supported by NOAA Climate Program Office AC4 program NA23OAR4310283 and NOAA cooperative agreement NA22OAR4320151.

1. H. Lee *et al.*, *Climate Change 2023: Synthesis Report. Contribution of Working Groups I, II and III to the Sixth Assessment Report of the Intergovernmental Panel on Climate Change* (The Australian National University, 2023).
2. E. G. Nisbet *et al.*, Methane mitigation: Methods to reduce emissions, on the path to the Paris agreement. *Rev. Geophys.* **58**, e2019RG000675 (2020).
3. E. J. Dlugokencky *et al.*, Observational constraints on recent increases in the atmospheric CH4 burden. *Geophys. Res. Lett.* **36**, L18803 (2009).
4. X. Lan, K. W. Thoning, E. J. Dlugokencky, Trends in globally-averaged CH4, N2O, and SF6 determined from NOAA Global Monitoring Laboratory measurements. https://doi.org/10.15138/P8XG-AA10. Accessed 6 May 2024.
5. O. A. Sherwood, S. Schwietzke, X. Lan, Global δ13C-CH4 source signature inventory 2020. *NOAA Global Monitoring Laboratory Data Repository* **10** (2021).
6. J. B. Miller *et al.*, Development of analytical methods and measurements of 13C/12C in atmospheric CH4 from the NOAA Climate Monitoring and Diagnostics Laboratory Global Air Sampling Network. *J. Geophys. Res. Atmos.* **107**, ACH-11 (2002).
7. S. Schwietzke *et al.*, Upward revision of global fossil fuel methane emissions based on isotope database. *Nature* **538**, 88–91 (2016).
8. S. Basu *et al.*, Estimating emissions of methane consistent with atmospheric measurements of methane and δ 13 C of methane. *Atmos. Chem. Phys. Discussions* **2022**, 1–38 (2022).
9. X. Lan *et al.*, Improved constraints on global methane emissions and sinks using δ13C-CH4. *Global Biogeochem. Cycles* **35**, e2021GB007000 (2021).
10. P. P. Tans, A note on isotopic ratios and the global atmospheric methane budget. *Global Biogeochem. Cycles* **11**, 77–81 (1997).
11. S. Peng *et al.*, Wetland emission and atmospheric sink changes explain methane growth in 2020. *Nature* **612**, 477–482 (2022).
12. Z. Qu *et al.*, Attribution of the 2020 surge in atmospheric methane by inverse analysis of GOSAT observations. *Environ. Res. Lett.* **17**, 094003 (2022).
13. M. Liu, L. Yang, A global fire emission dataset using the three-corner hat method (FiTCH). *Earth System Sci. Data Discussions* **2023**, 1–20 (2023).
14. J. R. Worden *et al.*, Reduced biomass burning emissions reconcile conflicting estimates of the post-2006 atmospheric methane budget. *Nat. Commun.* **8**, 2227 (2017).
15. Y. Zhao *et al.*, Influences of hydroxyl radicals (OH) on top-down estimates of the global and regional methane budgets. *Atmos Chem. Phys.* **20**, 9525–9546 (2020).
16. E. G. Nisbet *et al.*, Atmospheric methane: Comparison between methane's record in 2006–2022 and during glacial terminations. *Global Biogeochem. Cycles* **37**, e2023GB007875 (2023).
17. Z. Zhang *et al.*, Recent intensification of wetland methane feedback. *Nat. Clim. Chang.* **13**, 430–433 (2023).
18. L. Feng, P. I. Palmer, R. J. Parker, M. F. Lunt, H. Bösch, Methane emissions are predominantly responsible for record-breaking atmospheric methane growth rates in 2020 and 2021. *Atmos. Chem. Phys.* **23**, 4863–4880 (2023).
19. S. Michel *et al.*, Data in support of PNAS Brief Report [Data set]. National Oceanic and Atmospheric Administration. https://doi.org/10.15138/JQEV-PF31. Deposited 2 October 2024.

Downloaded from https://www.pnas.org by 178.205.55.180 on November 14, 2024 from IP address 178.205.55.180.